UpsFrac v1.0: An open-source software for integrating modelling and upscaling permeability for fractured porous rocks

Tao Chen[1,2], Honghao Sheng[1,2], Yu Zhang[1,2], Fengxin Kang[1,2,3]

[1]College of Earth Science and Engineering, Shandong University of Science and Technology, No. 579 Qianwangang Road, Qingdao, 266590, China
[2]Shandong Key Laboratory of Geothermal Clean Energy, 272000 Jining, China
[3]Shandong Provincial Bureau of Geology & Mineral Resources (SPBGM), No. 74 Lishan Road, Jinan, 250013, China

Correspondence to: Tao Chen (chentao9330@gmail.com)

Abstract. The efficient and accurate simulation of fluid flow and heat transport underground plays an important role in groundwater migration and geothermal resource prediction. Rock fractures are complex in geological settings, exhibiting multiple-scale properties with varied patterns under different geological conditions. Modelling and upscaling the permeability of fractured porous rocks are both important and sophisticated processes in numerical simulations. While existing tools like MRST offer upscaling capabilities, they often lack integrated workflows for automated uncertainty quantification and direct coupling between fractal-based DFM generation and flow-based upscaling within a single framework. In this study, we propose an integrated methodology for modelling and upscaling the permeability of fractured porous rocks and develop an open-source software, UpsFrac, to implement this approach. The software considers complex fracture geometries in discrete fracture models (DFM) that are created deterministically and stochastically. UpsFrac employs conforming grid-based DFM with explicit matrix-fracture coupling, ensuring higher accuracy for complex fracture networks. The software can characterize the complexity of fractured porous rocks, including power law (fractal) length distribution, correlations between fracture length and aperture, and the effects of rock matrix properties. The state-of-the-art upscaling method, the multiple-boundary fracture upscaling (MFU) method, is applied to calculate equivalent fracture permeability, which links the fine-scale discrete fracture model to the coarse-scale equivalent fracture model. The current implementation is 2D and MATLAB-based, built upon fracture modelling code ADFNE and reservoir simulation code MRST, which can easily run DFM ensembles for uncertainty analysis. The code is available in open repositories to encourage modelling and upscaling of complex fractured porous rocks, allowing users to develop their own routines within the current framework and benefiting a broader community.

1 Introduction

Fractures exist widely in geological settings and are caused mainly by changes in geomechanical stress, chemical erosion, and thermal stress (Gu et al., 2020; Gudmundsson, 2011; McDermott and Kolditz, 2006; Molnar et al., 2007; Zoback et al., 2003). These fractures can significantly influence the movement of fluids through rock formations, affecting groundwater

flow, contaminant transport, and the overall stability of geological formations (Cook et al., 2005; Marinos and Carter, 2018; Myers, 2012; Odling and Roden, 1997). In geothermal or petroleum reservoirs, fractures enhance the permeability and porosity, efficiently extracting heat and hydrocarbons (Ghassemi, 2012; Gong et al., 2021). Understanding the characteristics and behaviours of fractures is essential for reducing environmental risk, optimizing energy production, and implementing proper management strategies.

Quantitative analysis of reservoirs is essential for predicting sustainable production in geothermal or hydrocarbon systems, which mainly involves data collection, fractured porous rock modelling, upscaling, numerical simulation, and history matching (Andrews et al., 2019; HosseiniMehr et al., 2022; Liu and Reynolds, n.d.; Mejia et al., 2021; Neuman, 2005; Viswanathan et al., 2022). Discrete fractures occur at multiple scales, as illustrated in Fig. 1. Characterizing fractured porous media mainly involves gathering geological, hydrological, and geophysical data to obtain fracture and matrix properties within the reservoir, e.g., fracture orientation, length, density, and connectivity. Once the conceptual model of the fractured porous rock is built based on characterization, there are two primary numerical simulation approaches used to represent these fractures (Berre et al., 2018): the Discrete Fracture Model (DFM) or Discrete Fracture Network (DFN) and the Equivalent Fracture Model (EFM). The DFM approach explicitly represents each fracture within the reservoir, capturing the complexities of fluid flow and coupled processes. The EFM simplifies the representation by averaging the effects of fractures, making it computationally more efficient while still providing valuable insights. Upscaling techniques are required to calculate equivalent properties and construct a computationally efficient EFM based on the DFM. Accurate upscaling is particularly important for studying the heterogeneity and anisotropy of the reservoir and the existence of representative elementary volume (Wang et al., 2023), allowing for a better understanding of how these factors influence geothermal production (Gottron and Henk, 2021; Rajeh et al., 2019; Renard and Ababou, 2022). Modelling and upscaling discrete fracture models are prerequisites for the following numerical simulations and history-matching procedures.
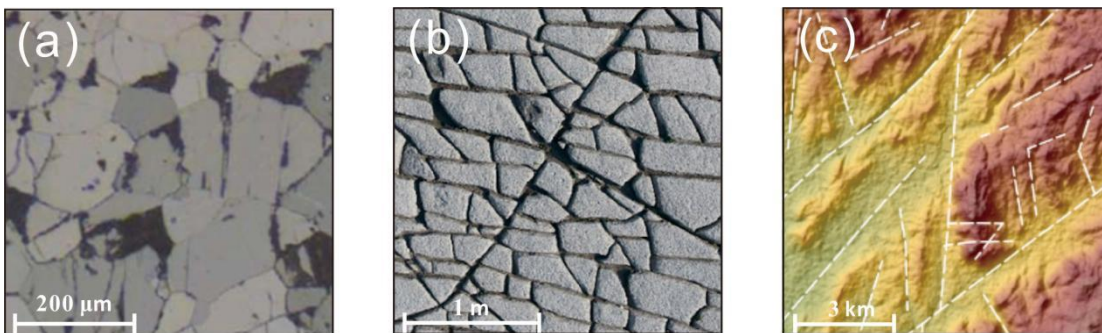
Figure 1: Multiple-scale fractures in geological settings. Adapted from Cheng and Wong (2018), Palamakumbura et al. (2020), and Weismüller et al., (2020).

Fractures are complex in their geometries and introduce uncertainty into models, primarily due to limited data availability and the influence of underground rock and fluid dynamics (MacQuarrie and Mayer, 2005; Srinivasan et al., 2018), which poses significant challenges in accurately characterizing and modelling fractured porous media. Numerous codes have been developed to advance the characterization and modelling of such media to address these issues. Hardebol and Bertotti (2013) developed DigiFract, a software solution that enables comprehensive fracture data collection from outcrops with greater efficiency than conventional surveying methods, enabling faster collection of larger and more accurate fracture datasets for better characterization of fractured rocks. Healy et al. (2017) developed FracPaQ, an open-source MATLAB™ toolbox designed for quantifying fracture patterns from two-dimensional images at multiple scales, such as thin section micrographs, geological maps, outcrop or satellite images. Alghalandis (2017) developed an open-source software ADFNE for stochastic modelling of discrete fracture networks in two- and three-dimensional applications. ADFNE provides a platform for visualizing and analyzing fracture networks, offering a valuable tool in fractured rock mechanics. Welch et al. (2020) developed DFN Generator v2.0, an innovative tool that simulates natural fracture network evolution based on geomechanical principles rather than stochastic methods, enabling more realistic modelling of fracture networks at kilometer scales. Ovaskainen (2023) developed the Python package fractopo, which provides tools for data validation and analysis of fracture trace observations digitized from base maps like drone images of outcrops or digital elevation models.

More recently, Borghini et al. (2024) introduced the Fracture Analyser, a simple and user-friendly Python tool, for the 2D analysis of fracture patterns in rock outcrops. The tool quantifies number, length, orientation, position, fracture density, etc., providing an efficient, flexible and accurate tool for the characterization and modelling of natural fractures. While several sophisticated tools exist for fractured porous rock modelling—such as PorePy (Keilegavlen et al., 2021) for discrete fracture-matrix simulations, DFNWorks (Hyman et al., 2015) for DFN flow and transport, SHEMAT-Suite (Keller et al., 2020) for coupled flow and heat transport, and OpenGeoSys (Kolditz et al., 2012) with its DFM modules, there remains a significant gap in linking such fracture geometric properties to the equivalent properties of the equivalent fracture model when doing numerical simulation. Few of these tools provide an integrated workflow that directly couples fractal DFM generation with flow-based permeability upscaling within a single framework. MRST (Wong et al., 2021) offers upscaling capabilities through embedded discrete fracture models (EDFM), but this approach uses non-conforming grids that may result in reduced accuracy for highly connected fracture networks. To the best of our knowledge, no open-source platform currently bridges fractal theory with practical permeability upscaling while enabling automated uncertainty quantification through ensemble-based analysis.

UpsFrac advances the state-of-the-art by providing one of the first integrated open-source solution bridging fractal theory and practical permeability upscaling. The platform unifies four key components: (1) fractal DFN generation combining deterministic and stochastic models with power-law distributions (Corral and González, 2019) and physically-based aperture-length correlations, capturing multi-scale characteristics of fractured systems; (2) direct coupling architecture

integrating DFM modelling with MFU (Chen et al., 2015) for permeability upscaling without file conversions, employing TPFA/MPFA schemes (Sandve et al., 2012) on conforming grids; (3) automated uncertainty quantification enabling efficient Monte Carlo analysis by streamlining workflows from fracture realization to equivalent properties calculation; and (4) an extensible MATLAB framework with modular architecture for incorporating new algorithms. This integrated approach streamlines uncertainty quantification, making large-scale stochastic analysis accessible to the research community. Table 1 positions UpsFrac relative to existing tools, highlighting its unique integrated workflow capability.

Table 1: Comparison of UpsFrac with existing fractured porous rocks modelling tools*

Feature	UpsFrac	PorePy	DFNWorks	MRST	OpenGeoSys
Programming Language	MATLAB	Python	C++/Python	MATLAB	C++
Open Source	Yes	Yes	Yes	Yes	Yes
Fracture modelling					
Stochastic DFN	Yes	Limited[1]	Yes	Yes	No
Power-law distribution	Yes	Limited[1]	Yes	Yes	No
Aperture-length correlation	Yes	Limited[1]	Yes	Yes	No
Flow Simulation					
DFM flow scheme	TPFA/MPFA	MPFA/TPFA/ MFD	FEM/TPFA	TPFA/MPFA	FEM
Matrix-fracture coupling	Yes	Yes	Yes	Yes	Yes
Fracture Upscaling					
Permeability upscaling	Yes	No	No	Yes	No
Integrated DFM-to-EFM workflow	Yes	No	No	Limited[1]	No
Automated uncertainty quantification	Yes	No	No	No	No

*TPFA: Two-Point Flux Approximation; MPFA: Multi-Point Flux Approximation; MFD: Mimetic Finite Difference; FEM: Finite Element Method; DFN: Discrete Fracture Network; DFM: Discrete Fracture Model; EFM: Equivalent Fracture Model.

[1]: Requires manual scripting.

2 Methodology and Theoretical Framework

UpsFrac software has three main components: modelling fractured porous rocks, fractured porous media upscaling and equivalent permeability visualization. For the fractured porous rock modelling part, the Matlab code ADFNE (Alghalandis, 2017) is required to supply basic functions for creating discrete fracture networks. For the flow-based upscaling procedure, the Matlab code MRST (Lie, 2019) is applied to solve the flow equations in the discrete fracture model. The detailed workflow of UpsFrac is shown in Fig. 2.
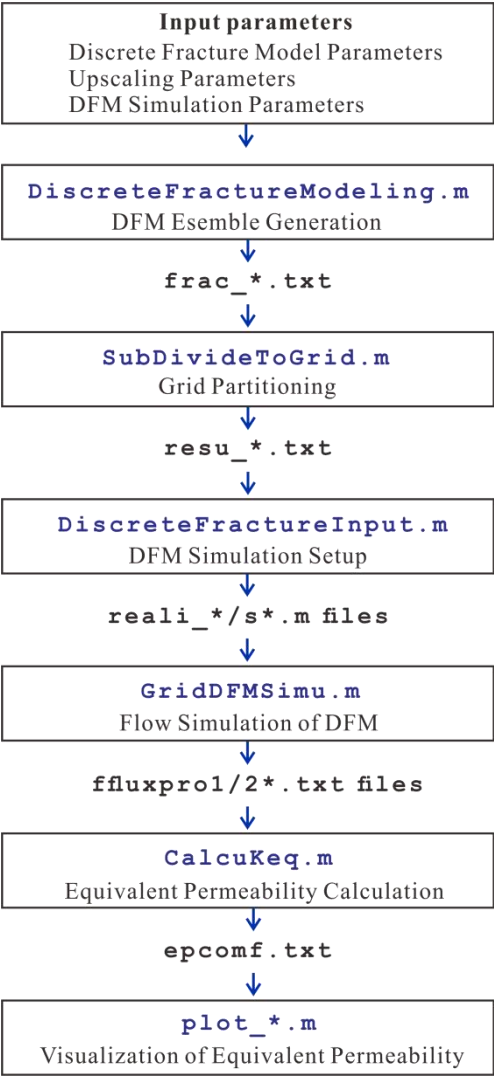
Figure 2: Implementation workflow of UpsFrac showing script execution sequence and data flow.

2.1 Modelling fractal fractured porous rock

The two-dimensional domain should be defined, e.g., as a rectangle with dimensions Lx and Ly, for modelling fractured porous rocks. The discrete fracture model can consider the discrete fracture network as well as the rock matrix. Fracture modelling includes both deterministic and stochastic approaches. After the fracture geometries are defined, the rest of the domain is filled with the rock matrix. The matrix can be characterized by permeability, porosity, etc.

For deterministic fractures, two endpoints, A(x1, y1) and B(x2, y2), and the fracture aperture should be defined for each fracture. Deterministic fractures are typically used for large-scale features such as faults or fractures with well-constrained geometries, which are important for modelling flow and heat transport.

For stochastic fractures, the discrete fracture network is determined by different geometrical properties (Bonnet et al., 2001), such as fracture length, aperture, position, and orientation (Xu and Dowd, 2010). The stochastic fracture is mainly based on the software ADFNE. Furthermore, UpsFrac is capable of modelling the truncated power-law length distribution which describes the fractal characteristics of natural fractures. The probability density function for the fracture length l can be written as (Corral and González, 2019; Hyman et al., 2016; Massart et al., 2010):

$$n(l) = \frac{\alpha-1}{l_{min}(1-(\frac{l_{min}}{l_{max}})^{\alpha-1})}(\frac{l_{min}}{l})^{\alpha}, \tag{1}$$

where l_{min} and l_{max} are the lower and upper bound of the fracture length, α, ranging from 1.3 to 3.5, is α power-law exponent influenced by the growth properties of fractures (Bonnet et al., 2001).

Furthermore, the fracture aperture, w, can be correlated to fracture length in UpsFrac by the following power law expression:

$$w = \gamma l^D, \tag{2}$$

where γ is the coefficient related to mechanical properties of fractured rocks and D denotes the correlation exponent, which signifies the mechanical interaction among closely positioned fractures. D may vary from 0.5 to 1 resulting from observations in the field. D = 0.5 represents complex open-mode fractures with a constant fracture toughness (Klimczak et al., 2010; Olson, 2003), while D = 1.0 occurs in faults and shear deformation bands under constant driving stress (Vermilye and Scholz, 1995).

Users can use the ADFNE framework to create stochastic realizations for fracture orientation, density, and location. Furthermore, users can develop their models to create stochastic fractures. All the fracture geometric parameters are defined in the modelling framework. The generated fracture geometries are exported in a standardized format that ensures seamless integration with subsequent upscaling procedures.

2.2 Upscaling permeability for fractured porous media

The upscaling procedure mainly involves finding the equivalent properties on coarse-scale grid blocks based on the information from fine-scale discrete fracture models. The first step is to divide the fracture domain into a Cartesian grid with $nx \times ny$ blocks. Each fracture is geometrically clipped at grid boundaries to identify its intersection segments within individual blocks. The fracture segments within each grid block are defined by their endpoint coordinates A (x1, y1) and B (x2, y2) and aperture values (Fig. 3), providing the geometric and hydraulic parameters necessary for flow simulation. It should be noted that the dimension of the Cartesian grid is $(Lx/nx) \times (Ly/ny)$; accordingly, all fracture endpoints are constrained within the individual grid block boundaries.
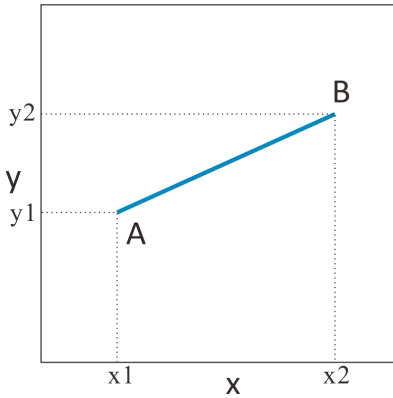
Figure 3: Schematic diagram of a fracture represented by endpoints A and B.

Next, the clipped fractures within each Cartesian grid form local discrete fracture networks for numerical simulation. The TPFA or MPFA schemes (Sandve et al., 2012) are employed to accurately model fluid flow in these highly heterogeneous media. Each grid block maintains identical dimensions and matrix properties, with only fracture geometries varying between blocks. The mesh refinement for both fractures and the matrix is adapted based on the local fracture density and complexity to ensure numerical accuracy.

Then, numerical simulations are conducted for each fractured grid block with pressure gradients applied along both x- and y-axes. The resulting flux distributions and pressure fields provide the necessary information for upscaling calculations. For grid blocks without fractures, the matrix permeability is directly assigned.

Subsequently, the MFU is applied to calculate the equivalent permeability for each grid block by using the previous simulation results. The MFU uses multiple boundary expressions to calculate flux. When the linear boundary conditions are applied along the x-axis, the flow rates along the x- and y-axes, q_x and q_y, are calculated on multiple boundaries:

$$q_\text{x} = \int_0^{l_y} v_\text{r} \cdot n_\text{x} \mathrm{d}y + \int_0^{l_x} v_\text{u} \cdot n_\text{x} dx + \int_0^{l_x} v_\text{l} \cdot n_\text{x} dx \ ,$$
$$q_\text{y} = \int_0^{l_x} v_\text{u} \cdot n_\text{y} dx + \int_0^{l_x} v_\text{l} \cdot n_\text{y} dx + \int_0^{l_y} v_\text{r} \cdot n_\text{y} dy \ ,$$

(3)

where l_x and l_y are dimensions of the Cartesian grid in the x- and y-directions, n_x and n_y are unit vectors along the x- and y-axes, v_r, v_u, and v_l denote the Darcy velocities on the right, upper, and lower boundaries.

Lastly, the coarse-scale equivalent permeability can be computed inversely based on the Darcy's law using the flux in the fine-scale discrete fracture model. The details of the MFU can be found in Chen et al. (2015). The resulting permeability tensor components (k_{xx}, k_{xy}, k_{yx}, k_{yy}) characterize the anisotropic flow behavior of each grid block.

2.3 Algorithmic Framework and Implementation

The upscaling workflow is designed as a modular framework consisting of five interconnected computational stages, each addressing specific mathematical and numerical challenges in fractured porous rocks characterization. Table 2 summarizes the computational stages, their mathematical formulations, and key parameters.

Table 2. Computational stages and mathematical framework of the UpsFrac workflow

Computational Stage	Mathematical Framework	Key Parameters	Primary Functions
DFM Generation	• Power-law distribution (Eq. 1) • Aperture-length correlation (Eq. 2)	• num_real: number of DFM realizations • n: number of fractures • α: power-law exponent • γ, D: aperture coefficients	Generate stochastic fracture realizations
Fracture-Coarse Grid Partitioning	• Geometric intersection algorithm • Boundary clipping	• dx, dy: coarse grid dimensions • tfrac: total fractures	Assign fractures to Cartesian blocks with boundary treatment
Simulation Setup	• TPFA/MPFA discretization • Cubic law	• Mesh refinement level • k_m: matrix permeability	Create DFM for flow equations
Flow Simulation	• Darcy's law • Orthogonal pressure gradients	•Boundary pressures •Solver type	Compute directional flux fields
Upscaling Calculation	• multiple boundary approach (Eq. 3) • Tensor assembly	• Flux decomposition angle • Physical constraint checks	Calculate equivalent permeability tensor

The framework incorporates key algorithmic features to ensure robust upscaling: (i) stochastic fracture generation with power-law length distributions and aperture-length correlations; (ii) geometric processing with boundary intersection detection and corner point adjustment to prevent mesh singularities; (iii) automatic mixed-dimension mesh generation integrating fracture and matrix elements; and (iv) batch processing of dual orthogonal flow problems. The upscaling employs directional flux decomposition through cosine transformations and validates permeability tensors to correct non-physical values from numerical errors. This modular architecture enables users to customize individual components—such as substituting alternative fracture generation models or numerical schemes—while maintaining framework compatibility, facilitating adaptation to diverse geological scenarios. The complete algorithmic pseudocode and implementation details are provided in Appendix A.1, with computational modules and data structures documented in Appendix A.2 for reproducibility.

2.4 Equivalent permeability visualization

The upscaled equivalent permeability tensors are analyzed and visualized to characterize flow behavior in fractured porous rocks. The resulting equivalent permeability is a full tensor form and is not inherently symmetric for fractured rocks (Chen et al., 2016; Zijl and Stam, 1992). When a symmetric tensor is required, a symmetric permeability tensor can be obtained by averaging the off-diagonal components. Using the upscaling results, the distribution of permeability tensor components (k_{xx}, k_{xy}, k_{yy}) can be visualized to characterize spatial heterogeneity and anisotropy. In addition, the equivalent permeability tensor of each grid block can also be plotted as an ellipse to visualize the directional permeability. Furthermore, to analyze the statistical properties of the equivalent permeability, histogram analysis of the permeability components is performed, which is important for building stochastic fields of equivalent permeability (Fiori et al., 2015) and supporting uncertainty quantification in reservoir modelling.

3 Validation

3.1 Fracture with power law length distribution

For modelling the fracture length with power law distribution, the cut-off power law is applied to create fracture length. For fractures with length l ranging from l_{min} to l_{max}, the power law distribution can be expressed as in equation (1). The power law distribution for fracture length is created using the rndm_powerlaw function. The values of l_{min}, l_{max}, power-law exponent α and fracture number N should be determined. For instance, when l_{min}=10 m, l_{max}=1000 m, α=2.5, and N=500, the histogram of stochastically generated fracture length is plotted in Fig. 4, showing a typical power-law decay pattern with most fractures concentrated at smaller lengths. When fitting the stochastically generated data with the maximum likelihood estimation method, the fitted α is 2.52, close to the input alpha 2.5. The Kolmogorov-Smirnov statistic is 0.032, indicating that the software UpsFrac generates the data set and agrees with the fitted power-law distribution.
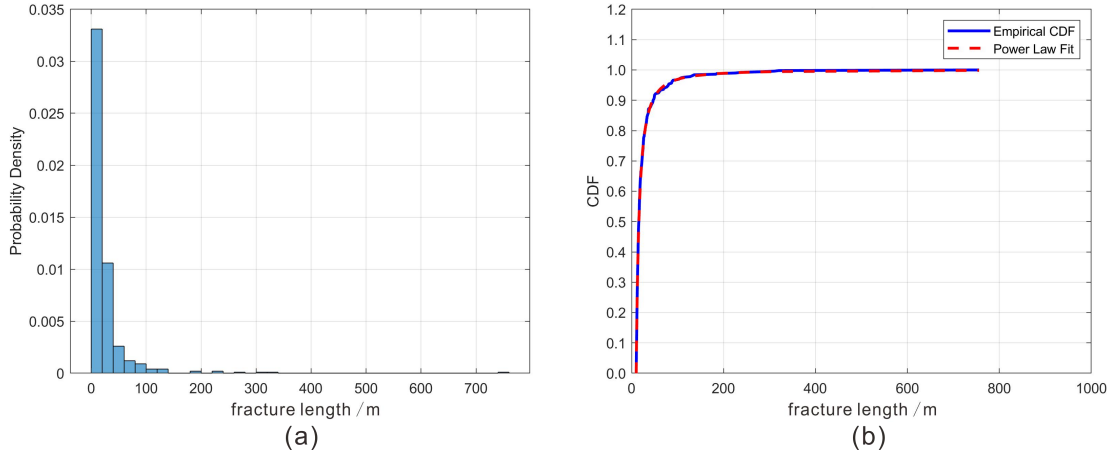
Figure 4: (a) Histogram of power law distribution, (b) Cumulative Distribution Function (CDF) of created data and fitted power law.

3.2 Equivalent fracture permeability with varied aperture

215   To validate the accuracy of UpsFrac's upscaling methodology, we compare the calculated equivalent permeability against analytical solutions for a single fracture embedded in a low-permeability matrix. The validation setup consists of a 2 m × 2 m domain containing a 2 m horizontal fracture at y = 1 m spanning the entire domain width (Fig. 5a). The matrix permeability k_m = 9.87×10^{-16} m², and the fracture permeability k_f varies based on aperture according to the cubic law. Linear pressure boundary conditions are applied on all four boundaries: left boundary (x = 0) with P = 2 Pa, right boundary (x = 2) with P =

220   0 Pa, and top/bottom boundaries with P = 2 - x Pa, representing a unit gradient flow field.
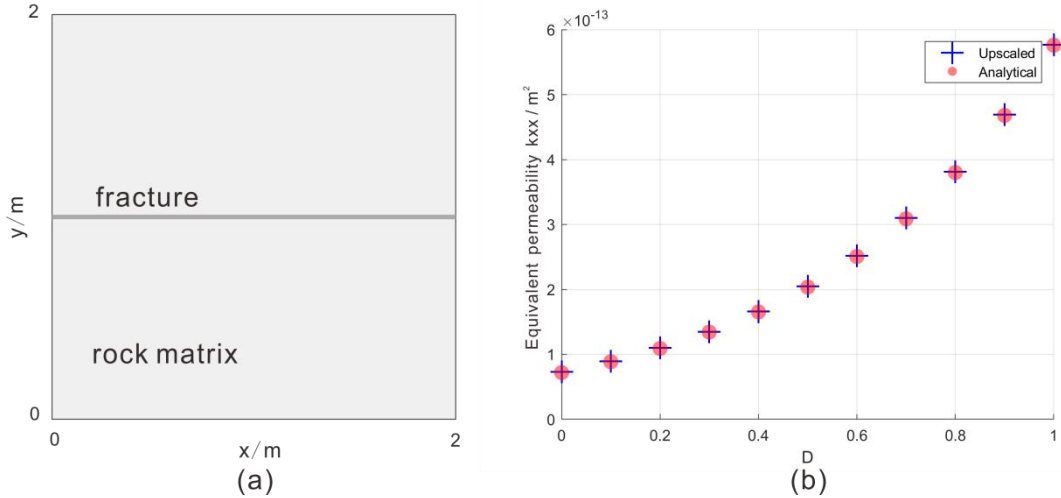
Figure 5: Validation of upscaling methodology for a single horizontal fracture: (a) model geometry showing fracture and matrix configuration, and (b) comparison of upscaled and analytical equivalent permeability for varied aperture values.

The analytical solution for equivalent permeability k_{xx} under parallel flow assumption between fracture and matrix is derived from flow equivalence principle (Snow, 1969). For the single-fracture case, this can be simplified to:

$$k_{xx} = k_m \times (1 - w/\Delta y l_y) + k_f \times w/\Delta y l_y, \qquad\qquad (4)$$

where $k_f = w^2/12$ based on the cubic law, and Δy is the domain height in the y-direction ($\Delta y = l_y$ for this single-block validation case).

We tested the upscaling accuracy by varying fracture aperture with correlation exponent D from 0 to 1 ($\gamma = 1.2 \times 10^{-4}$). The equivalent permeability calculated by UpsFrac ranged from 0.7×10^{-13} m² to 5.8×10^{-13} m², showing excellent agreement with the analytical solution (maximum relative error < 1%, Fig. 5b). The MFU enables accurate handling of fractures at arbitrary angles (Chen et al., 2015), critical for complex networks with non-aligned fractures. The modular framework allows easy incorporation of alternative aperture models, including rough fractures (see Section 5.1).

3.3 Numerical accuracy and sensitivity analysis

The numerical performance of the upscaling methodology is evaluated through three complementary analyses: grid convergence studies to establish discretization requirements, parametric investigation of fracture-matrix permeability contrasts, and orientation-dependent error assessment. These analyses collectively demonstrate the method's accuracy and robustness for practical applications.

3.3.1 Grid convergence studies

To assess the numerical accuracy and grid sensitivity of the upscaling methodology, systematic convergence studies were performed on a representative 2D fractured domain containing a single horizontal fracture. The computational domain measures 2 m × 2 m with the fracture positioned at y = 1 m, spanning the entire domain width. The fracture aperture was set to 120 μm with a permeability of 1.2×10^{-9} m² based on the cubic law, while the surrounding rock matrix has a permeability of 9.87×10^{-16} m². This configuration represents a fracture-matrix permeability contrast of approximately six orders of magnitude, representing highly conductive fracture systems commonly encountered in crystalline rocks and tight formations. Six progressively refined grids were employed with spacings ranging from h = 1.0 m (2×2 grid) to h = 0.025 m (80×80 grid), enabling a comprehensive evaluation of grid-dependent effects on the computed equivalent permeability tensor (Fig. 6).
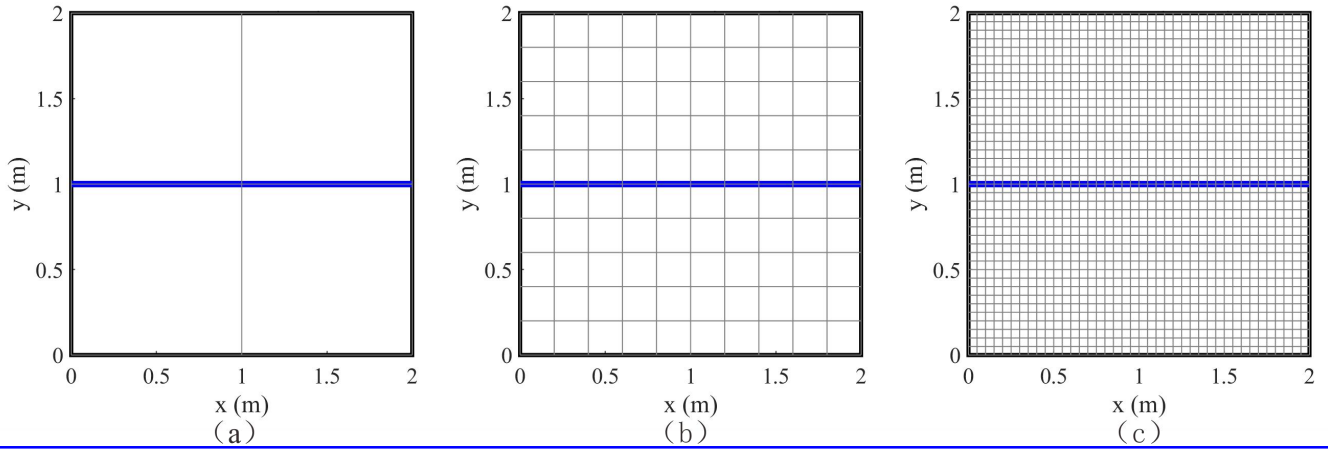
Figure 6: Visualization of selected grid refinement levels showing the progressive mesh resolution from (a) h = 1.0 m (2×2), (b) h = 0.2 m (10×10), to (c) h = 0.05 m (40×40) with the horizontal fracture indicated in blue.

The upscaling procedure demonstrates excellent convergence behavior with systematic grid refinement (Fig. 7a). The computed equivalent permeability values range from 7.2500 × 10⁻¹⁴ m² for the coarsest grid to 7.2975 × 10⁻¹⁴ m² for the finest resolution, converging monotonically. The relative errors reported here are computed against the finest grid solution (h = 0.025 m) as the reference to assess pure grid convergence behavior. Even the coarsest 2×2 grid achieves a relative error of only 0.65%, while grids with h ≤ 0.2 m maintain errors below 0.13%. The log-log error analysis (Fig. 7b) confirms rapid convergence with decreasing grid spacing. Notably, the h = 0.1 m grid (20×20) provides accuracy within 0.052% while using only 6% of the computational cells compared to the finest 80×80 grid. These results establish that grid spacings of 0.1-0.2 m offer optimal balance between computational efficiency and numerical accuracy for practical applications.
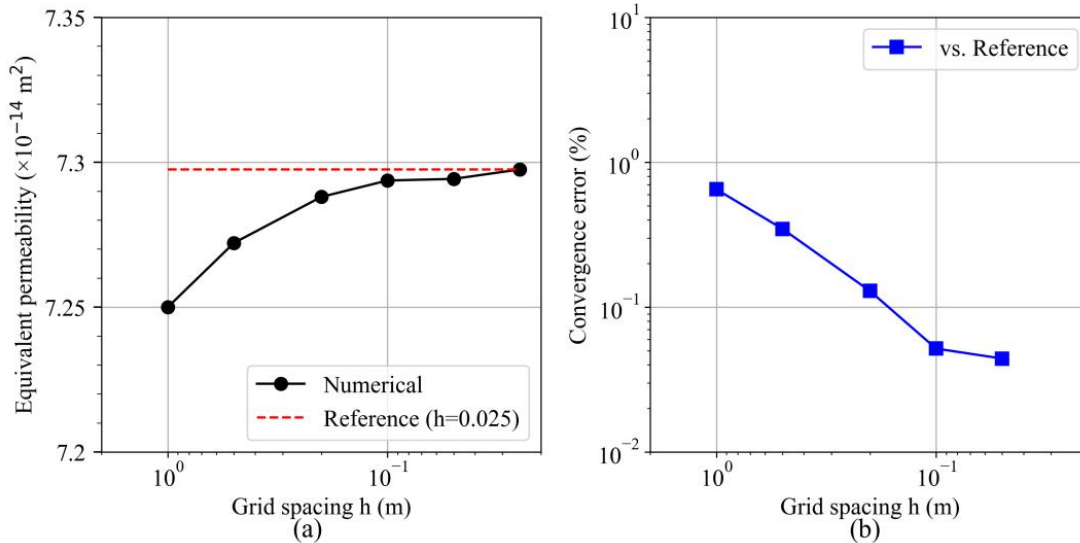
Figure 7: Grid convergence of equivalent permeability showing (a) permeability values; (b) relative error.

3.3.2 Fracture-Matrix permeability contrast

The influence of fracture-matrix permeability contrast on upscaling accuracy was investigated using a 2 m × 2 m domain with a single horizontal fracture. The matrix permeability, k_m, was fixed at 9.87×10^{-16} m², while fracture aperture varied from 1.09 to 108.83 μm, yielding fracture permeabilities, k_f, from 9.9×10^{-14} to 9.87×10^{-10} m² based on the cubic law. This creates permeability contrasts spanning four orders of magnitude ($k_f/k_m \approx 10^2$ to 10^6), encompassing conditions from tight formations to highly conductive systems. The equivalent permeability tensor was computed using UpsFrac and compared against analytical solutions from parallel flow theory.

(a)   (b)
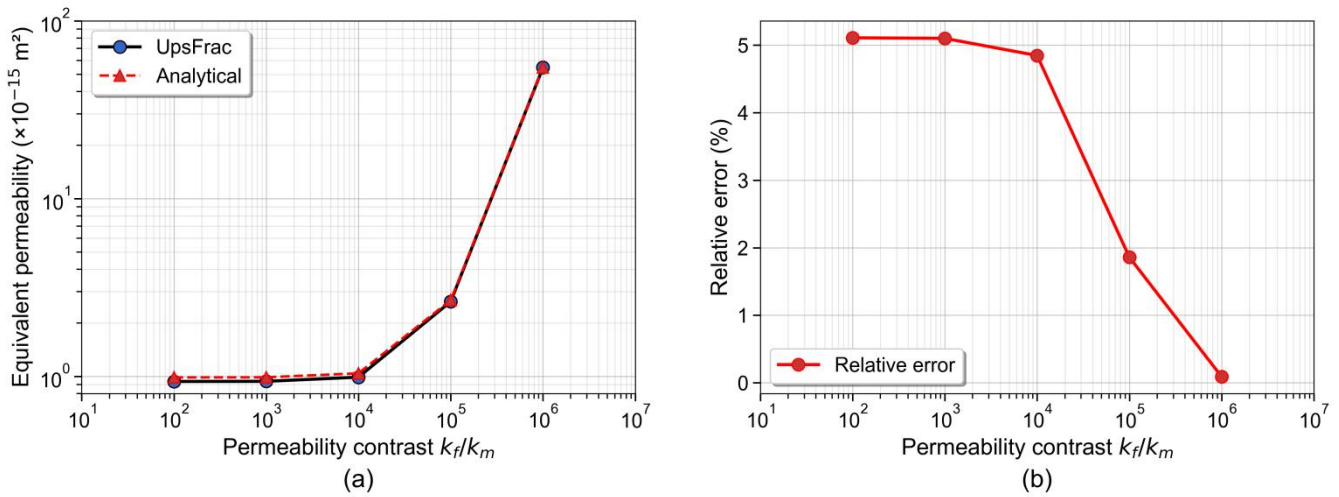
Figure 8: Comparison of upscaled equivalent permeability between UpsFrac numerical solutions and analytical reference values for different fracture-matrix permeability contrasts (a) comparison of equivalent permeability; (b) relative error analysis.

Figure 8a demonstrates excellent accuracy across the entire contrast spectrum. The upscaled permeability values closely track analytical solutions, capturing the transition from matrix-dominated ($k_f/k_m < 10^3$) to fracture-dominated ($k_f/k_m > 10^5$) flow regimes. At low contrasts, equivalent permeability approximates the matrix value; at high contrasts, it reaches several orders of magnitude above the matrix. The numerical solutions consistently capture this nonlinear scaling with remarkable fidelity.

Figure 8b reveals consistently low relative errors across all contrasts, with a mean error of 3.40%. The maximum error (5.11%) occurs at low contrasts where fracture contribution is minimal, decreasing to <0.1% for high-contrast systems. This trend confirms UpsFrac's suitability for highly fractured systems requiring accurate preferential flow representation. The robust performance across diverse contrasts validates the upscaling formulation for applications ranging from tight shales to karstified carbonates.

3.3.3 Orientation-dependent error

To evaluate the sensitivity of the upscaling methodology to fracture orientation relative to the computational grid, a comprehensive analysis was conducted using a single fracture rotated at angles of 0°, 30°, 45°, 60°, and 90° within a 2 m × 2 m domain (Fig. 9). The fracture maintains a constant aperture of 120 μm, embedded in a matrix with permeability of 9.87×10^{-16} m². For each orientation, the full permeability tensor was computed using UpsFrac and compared against analytical solutions obtained through coordinate transformation of the reference configuration. For a fracture with azimuth θ, the equivalent permeability tensor can be written as:

$$k(\theta) \equiv \begin{bmatrix} k_{xx} & k_{xy} \\ k_{yx} & k_{yy} \end{bmatrix} \equiv \begin{bmatrix} k_x^* \cos^2\theta + k_y^* \sin^2\theta & (k_x^* - k_y^*)\cos\theta \cdot \sin\theta \\ (k_x^* - k_y^*)\cos\theta \cdot \sin\theta & k_x^* \sin^2\theta + k_y^* \cos^2\theta \end{bmatrix}, \tag{5}$$

where k_x^* and k_y^* are the equivalent permeability tensor components in the x- and y-directions for a horizontal fracture ($\theta = 0°$), respectively. Here, k_x^* can be calculated from Eq. 4, and $k_y^* \approx k_m$ since a single fracture aligned with the x-axis has negligible impact on the y-direction permeability.
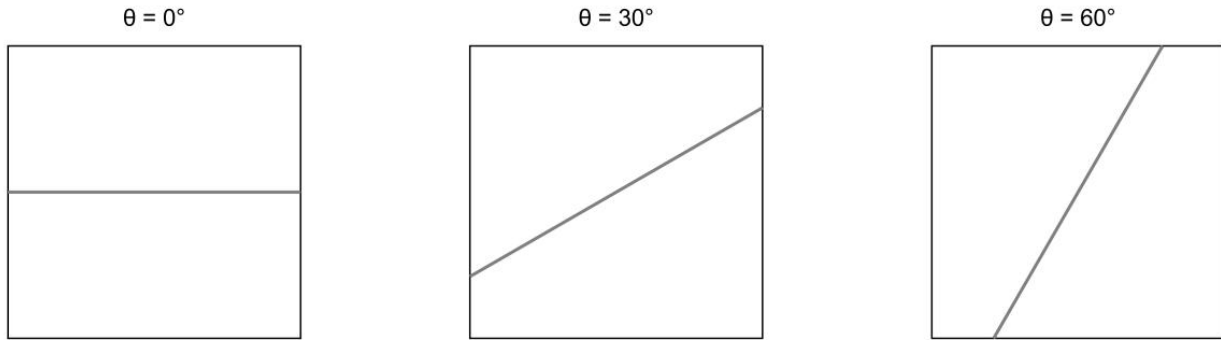
Figure 9: Representative fracture orientations at (a) 0°, (b) 30°, and (c) 60°.

Figure 10a demonstrates the evolution of permeability tensor components with fracture orientation. The diagonal components k_{xx} and k_{yy} exhibit sinusoidal variation between fracture-dominated (7.3×10^{-14} m²) and matrix-dominated (9.87×10^{-16} m²) directions, while k_{xy} peaks at 45° where fracture contribution is equally distributed between the x- and y-directions. The UpsFrac solutions closely match analytical curves for this single fracture configuration, achieving excellent agreement with mean relative errors of 1.10%, 3.15%, and 0.07% for k_{xx}, k_{yy}, and k_{xy}, respectively. The accurate calculation of off-diagonal components is particularly important when sparse fractures are not aligned with the coordinate axes.
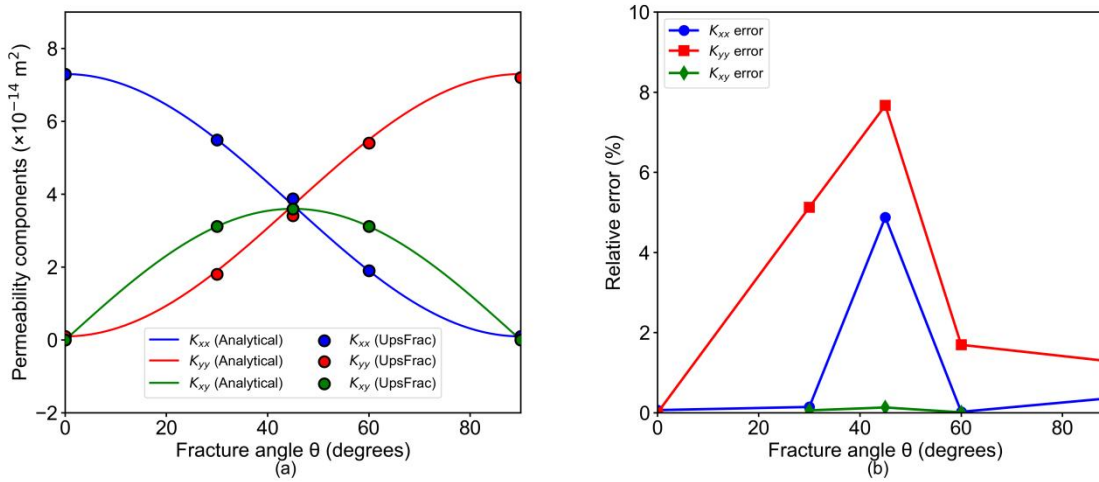
Figure 10: Orientation-dependent validation of upscaled permeability: (a) permeability tensor components as functions of fracture orientation angle; (b) relative errors between UpsFrac numerical solutions and analytical reference values.

Figure 10b reveals the maximum error (7.67%) occurs at 45° orientation. At 45° orientation, fracture endpoints naturally terminate near domain corner nodes, creating ambiguity in boundary condition assignment. To maintain numerical stability and avoid singular matrix configurations, slight geometric adjustments are required to displace fracture endpoints away from exact corner positions. Despite this localized issue, overall accuracy remains excellent with errors below 5% for most orientations. These results validate that UpsFrac reliably handles arbitrarily oriented fractures without grid alignment, essential for modelling complex natural fracture networks.

4 Software application

4.1 Discrete fracture modelling and upscaling application

The modelling and upscaling procedure is applied to a real-scale problem by using UpsFrac. The model domain is 1000 m × 1000 m. The domain contains both large-scale fractures (faults) and small-scale fractures, referring to the measured data in the field (Massart et al., 2010). The fracture network contains both deterministic fractures and stochastically generated fractures. The deterministic fractures include three fractures with an aperture of 0.001 m. The stochastic fracture length follows a power law distribution, with l_{min}=10 m, l_{max}=1000 m, N=200, and α=2.5. Fracture orientation follows Fisher distribution with κ =0, meaning the fracture orientation is randomly distributed. Fracture location follows uniform distribution. In this study, the aperture is correlated with fracture length with γ of 2.3×10^{-5} and D of 0.5 according to the field data (Schultz and Soliva, 2012). The above geometric data are input parameters for the fracture modelling module. The

rock matrix permeability is homogeneous and isotropic with 9.87×10^{-16} m². One realization of the discrete fracture model is shown in Fig. 11.

325
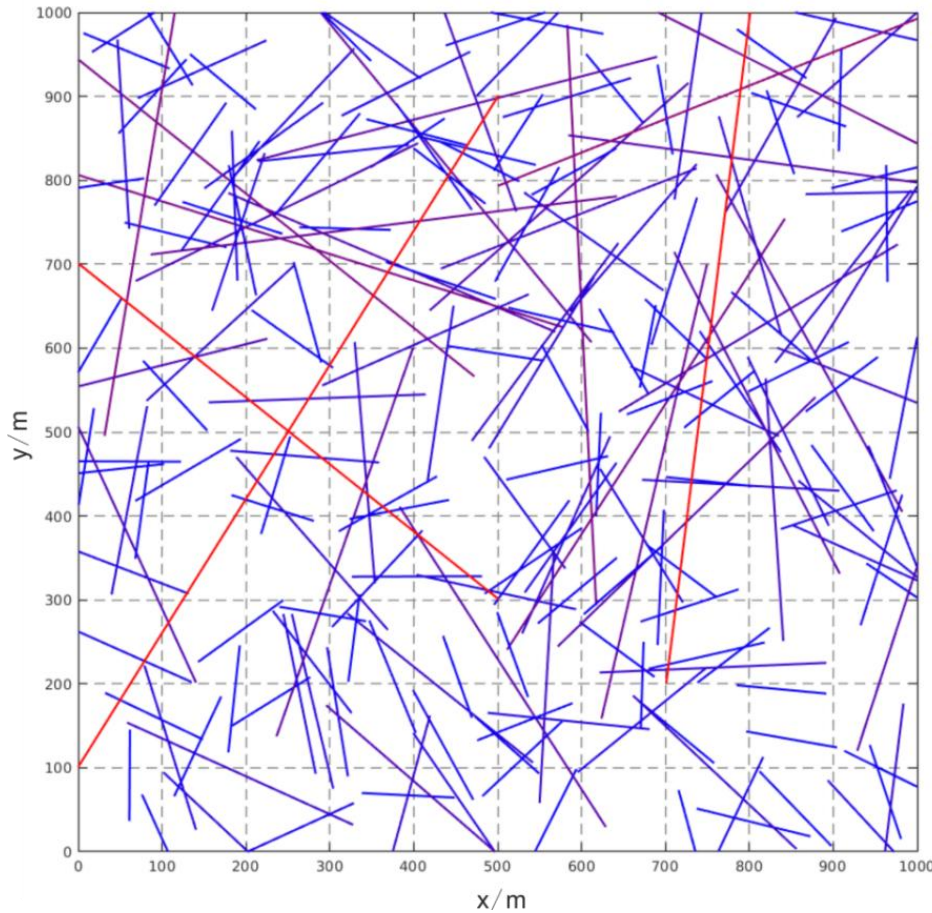
Figure 11: Discrete fracture model generated by UpsFrac. Blue denotes a low aperture, red denotes a high aperture, and the dashed line denotes the grid blocks on a coarse scale.

The grid block size for upscaling is 100 m×100 m, which is the input parameter for the grid subdivision module. Each grid
330 contains 3-9 fractures clipped by the grid boundaries. For the numerical simulation of each grid, the unstructured mesh size for the rock matrix is 5 m, and for fracture, it is 3.3 m. After simulating fluid flow in all grid blocks, the required information for upscaling is calculated. Through the upscaling calculation module, the equivalent permeability for each grid block is calculated.
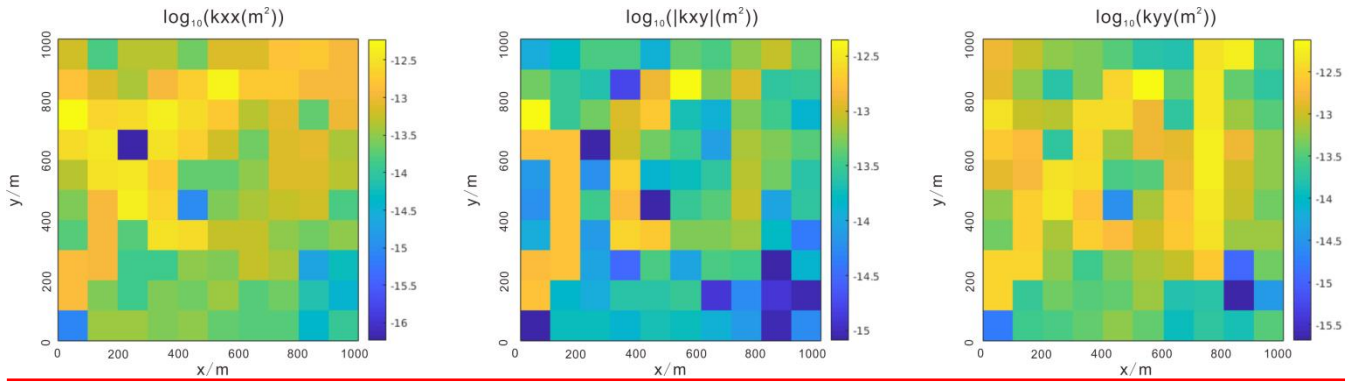
Figure 12: Equivalent permeability distribution of grid blocks on a coarse scale.

The resulting equivalent permeability distribution is visualized in Fig. 12. The equivalent permeability distribution shows that it is highly correlated with the fracture network geometries of fractures (Fig. 12). The anisotropy in equivalent permeability components is controlled by the fracture orientation distribution.
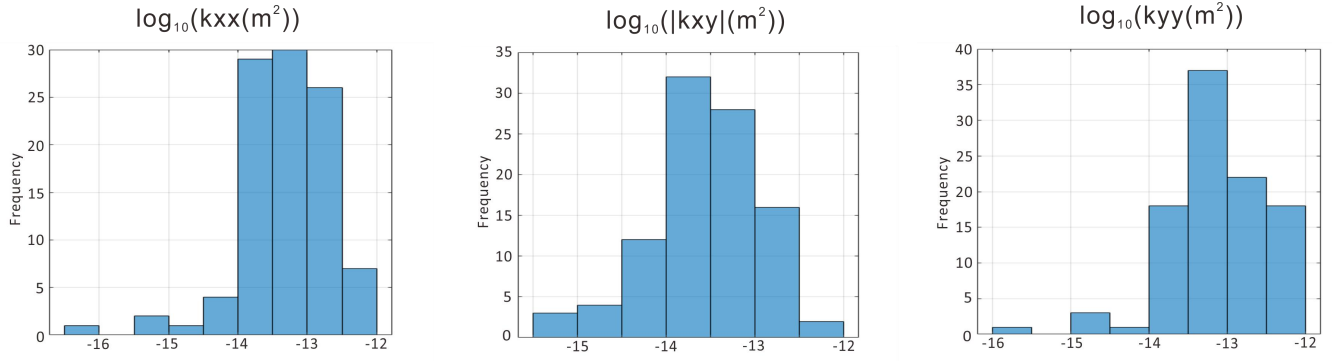
Figure 13: Histograms of upscaled equivalent permeability components.

The histograms of different components of equivalent permeability are plotted in Fig. 13. They show that all components k_{xx}, k_{xy}, and k_{yy} follow a log-normal distribution. For k_{xy}, it can be positive and negative; we use the absolute value here for plotting. For k_{xx} and k_{xy}, the shapes of the histograms are similar. The results indicate that even though the spatial distribution is different, the statistical properties of k_{xx} and k_{xy} are similar. This is mainly due to the random distribution of fracture orientations, i.e., without a preferable orientation. For k_{xy}, it is slightly lower than k_{xx} and k_{xy}; this is consistent with the positive-definite nature of the permeability tensor (Lang et al., 2014).
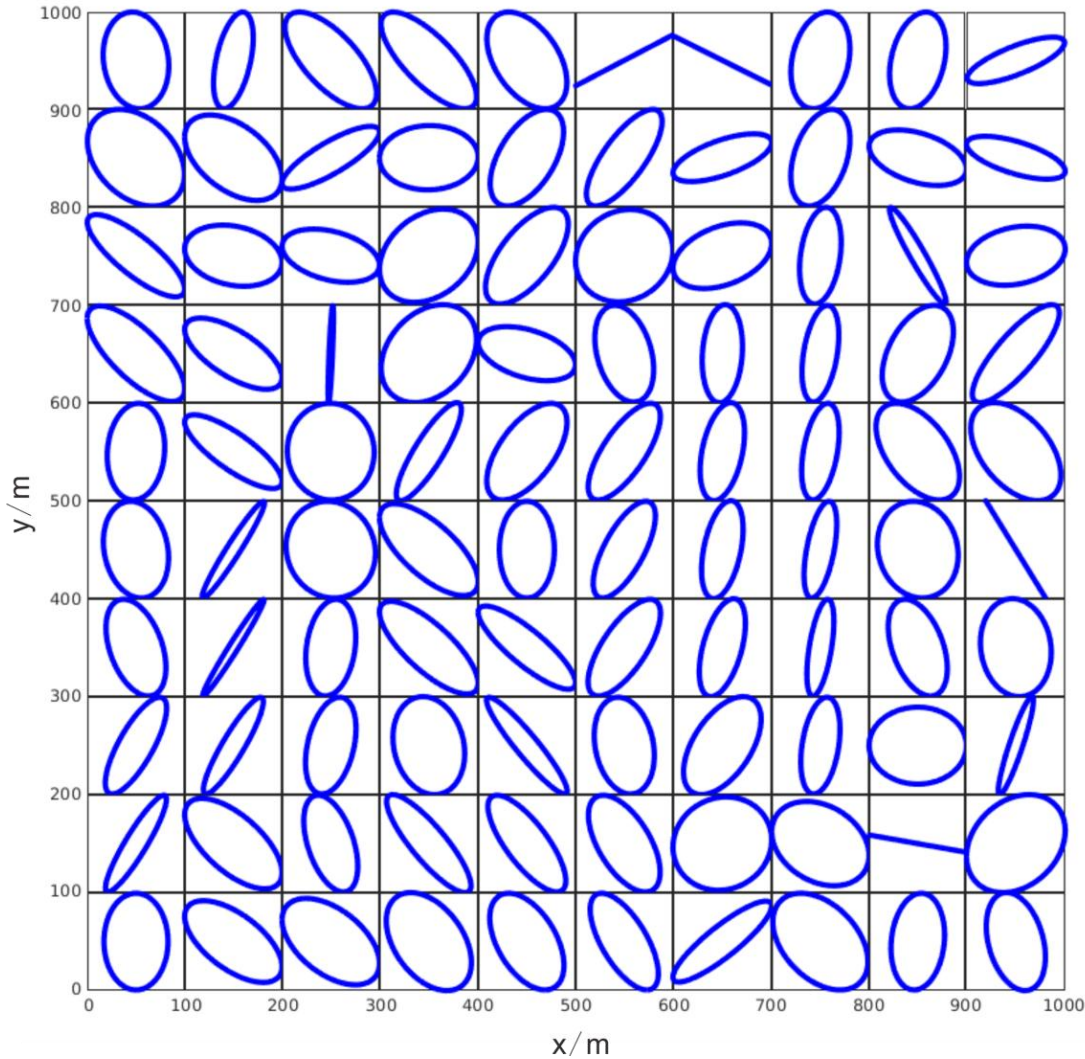
The permeability tensor can be visualized using the ellipses. The permeability ellipses for all grid blocks are plotted in Fig. 14. They show that the long axes of an ellipse follow the fracture orientations (Fig. 11), especially for the grid with a few

355 large fractures having high permeability (e.g., the grid block near the lower left corner of the model). The consistency between the upscaled permeability tensor ellipses and the fracture network geometries indicate that the upscaling code UpsFrac yields reasonable and accurate results. These results can be used to characterize the permeability of the fractured porous rocks and serve as input to equivalent fracture models.

4.2 Comparison between upscaled EFM and DFM for fractured geothermal systems

A two-dimensional fractured geothermal system model was developed to evaluate the computational performance and accuracy of the EFM upscaling approach (Fig. 15). The model simulates a 500 m × 500 m geothermal reservoir with a doublet injection-production well configuration (150 m spacing), where cold water at 40 °C is continuously injected at the injection well and produced at the production well, both at 1 L/s. The domain is initialized at 80°C and 20 MPa, with no-flow and adiabatic boundary conditions representing sealed cap and base rocks. The rock matrix has typical geothermal reservoir properties: permeability of 9.87×10^{-16} m², 1% porosity, density of 2600 kg/m³, specific heat of 950 J/(kg·K), and thermal conductivity of 3.0 W/(m·K). The fractures feature a 500 μm mean aperture with 100% porosity. Fluid properties include density of 1000 kg/m³, viscosity of 0.001 Pa·s, specific heat of 4200 J/(kg·K), and thermal conductivity of 0.65 W/(m·K), representing typical values for fractured geothermal systems.
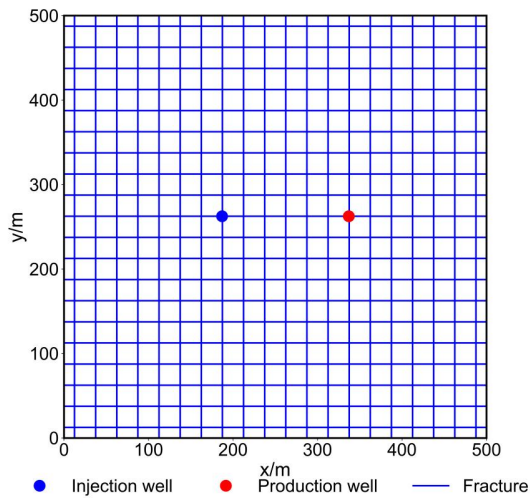
Figure 15: Conceptual model of the field-scale geothermal doublet system with 500 m × 500 m domain and 150 m well spacing.

The DFM and EFM models were constructed using different meshing strategies to enable direct performance comparison (Fig. 16). For the DFM model, GMSH was employed to generate an unstructured mesh with 13,414 nodes and 30,006 elements, comprising 3,820 line elements for the fracture network and 26,186 triangular elements for the rock matrix. In contrast, the EFM model utilized a structured 20×20 grid with uniform cell dimensions of 25 m × 25 m, resulting in 400 grid cells. The upscaling procedure using UpsFrac yielded homogeneous equivalent permeabilities of $k_{xx} \approx 4.116 \times 10^{-13}$ m² and $k_{yy} \approx 4.100 \times 10^{-13}$ m², with zero off-diagonal terms ($k_{xy} = k_{yx} = 0$), indicating isotropic permeability characteristics and alignment of the principal permeability directions with the coordinate axes.

(a)   (b)
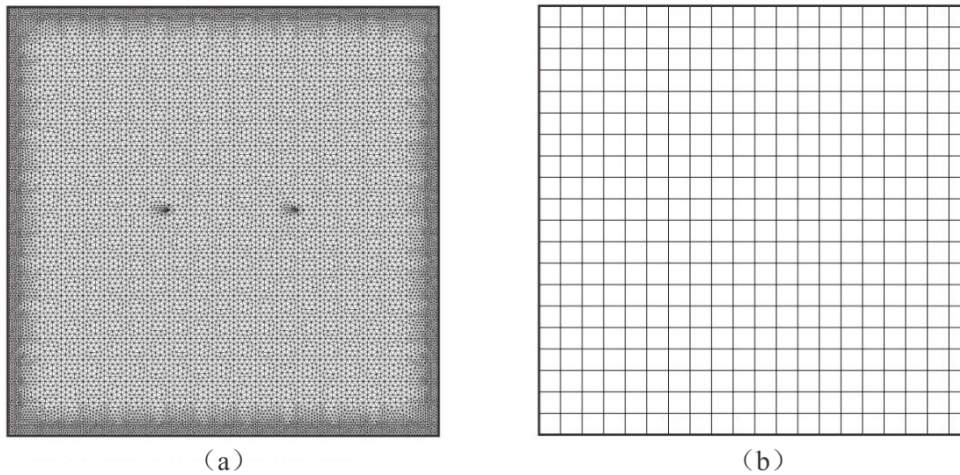
Figure 16. Mesh discretization for (a) DFM model with 13,414 nodes and (b) EFM 20×20 structured grid.

380   Both EFM and DFM were employed to solve the coupled flow and heat transfer processes using SHEMAT-Suite and OpenGeoSys, respectively. The validation results demonstrate excellent agreement between the upscaled EFM model and the high-fidelity DFM benchmark (Fig. 17). Temperature breakthrough curves at the production well over 30 years show mean relative error of approximately 0.2%, achieved with only 400 coarse grid cells compared to the 13,414-node DFM discretization, confirming the upscaling approach's high accuracy and robustness.

385
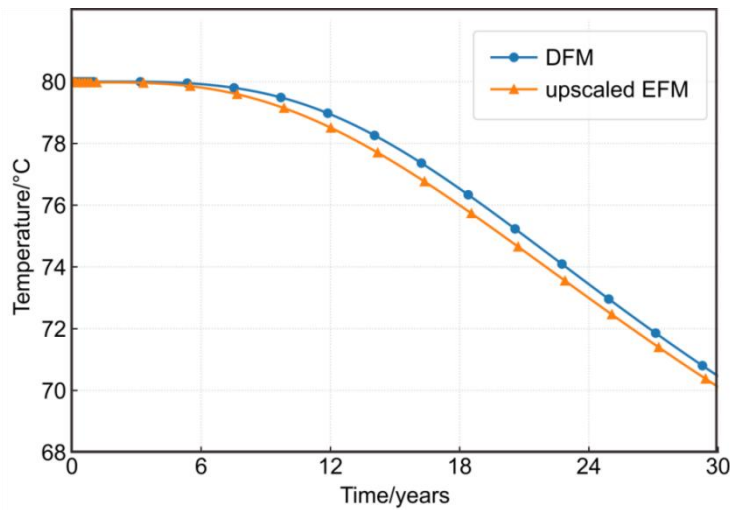
Figure 17: Temperature breakthrough curves comparing DFM reference and EFM upscaled models over 30 years.

The computational performance analysis reveals substantial efficiency gains of the EFM approach (Fig. 18). The EFM upscaling process consists of four stages: Fracture-Coarse Grid Partitioning (0.186 s, 0.13 MB), Simulation Setup (28.659 s, 3.02 MB), Flow Simulation (71.245 s, 13.03 MB), and Upscaling Calculation (49.650 s, 0.67 MB), totaling 149.74 s for the upscaling process. The subsequent EFM simulation requires 540 s and 7.48 MB. In contrast, DFM using OpenGeoSys requires meshing (21.45 s, 139.41 MB) and simulation (2081 s, 75.30 MB). The complete EFM workflow required only 689.74 s versus 2102.45 s for DFM—a 67% reduction. Total memory usage decreased from 214.71 MB to 24.33 MB—an 89% reduction. These benchmarks were conducted on an Intel Core i5-9300H system with 8 GB RAM. The results confirm that the EFM upscaling methodology achieves both computational efficiency and numerical accuracy (~0.2% relative error), making it particularly suitable for large-scale fractured reservoir simulations. However, accuracy may decrease for complex fracture networks with highly irregular geometries or dense intersection patterns, where validation against fine-scale DFM solutions or field data becomes essential.
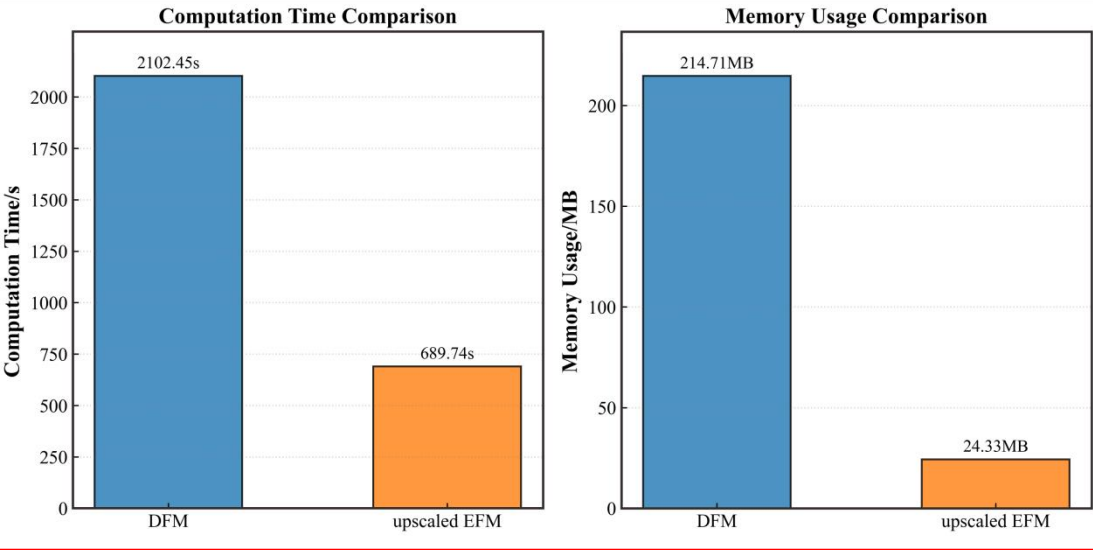
Figure 18: Computational performance comparison showing runtime and memory usage for DFM and EFM simulations.

4.3 Stochastic Ensemble Analysis and Uncertainty Quantification of Upscaled Permeability

To quantify uncertainty in upscaled properties arising from stochastic DFN realizations, we performed Monte Carlo analysis with 100 independent realizations using the same geometric parameters, matrix properties, and grid configuration as described in Section 4.1. The ensemble analysis reveals distinct distribution characteristics for the upscaled permeability tensor components. The diagonal components (k_{xx} and k_{yy}) exhibit approximately log-normal distributions as confirmed by

Q-Q plot analysis, while the off-diagonal component (k_{xy}) shows normal distribution characteristics (Fig. 19). The mean upscaled permeability values across all realizations and grid cells are k_{xx} = 1.334×10⁻¹³ m², k_{yy} = 1.325×10⁻¹³ m², and k_{xy} = 6.685×10⁻¹⁶ m². The coefficients of variation reveal moderate variability for diagonal components (k_{xx}: CV=0.889, k_{yy}: CV=0.910) and significantly higher uncertainty for the off-diagonal component (k_{xy}: CV=106.288), primarily due to its very small mean value (6.685×10⁻¹⁶ m²) relative to its standard deviation (7.105×10⁻¹⁴ m²), resulting in an amplified coefficient of variation.
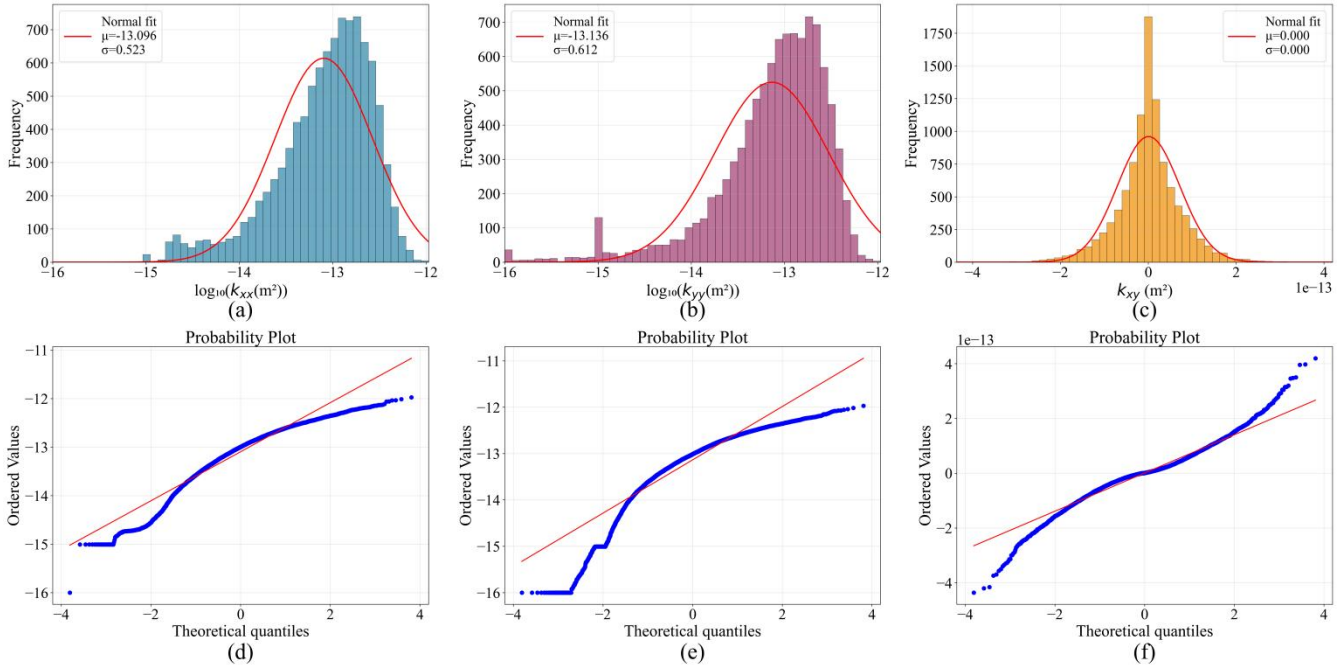
Figure 19: Distribution characteristics of upscaled permeability tensor components: (a,c,e) histograms and (b,d,f) Q-Q plots for Kxx, Kyy, and Kxy respectively.

Convergence analysis demonstrates robust statistical behavior of the ensemble approach. The mean values of diagonal permeability, k_{xx} and k_{yy}, components stabilize after approximately 50-60 realizations, achieving relative errors below 5% compared to the full 100-realization ensemble, all converging to 1.33×10⁻¹³ (Fig. 20). The off-diagonal component k_{xy} converges to near-zero values. Due to the lack of pronounced directional preference in the fracture orientation distribution, and additionally, the relatively small magnitude of k_{xy} values leads to slightly larger convergence relative errors compared to k_{xx} and k_{yy}. This convergence pattern indicates that 50 realizations provide sufficient statistical reliability for practical uncertainty quantification, offering guidance for balancing computational cost with accuracy requirements. The rapid convergence of ensemble statistics validates the Monte Carlo approach for capturing the stochastic variability inherent in fractured porous rocks.
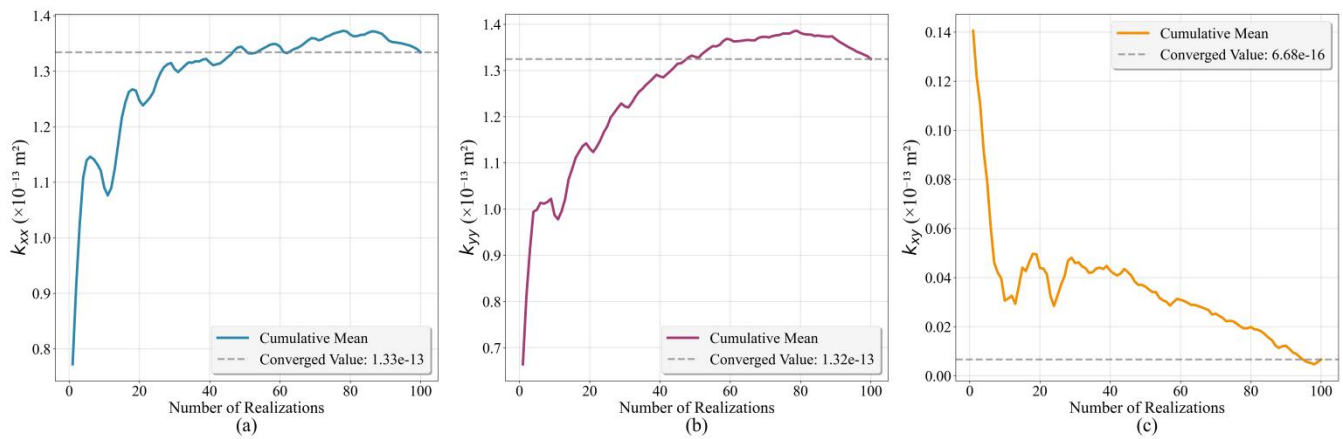
Figure 20: Convergence of ensemble mean values for upscaled permeability components: (a) kxx, (b) kyy, and (c) kxy.

The computational performance analysis reveals that the complete workflow—from fracture network generation to permeability upscaling—requires approximately 108 minutes total computational time for 100 realizations (1.08 minutes per realization) with peak memory usage of 8.2 GB. These benchmarks were conducted on a workstation equipped with an Intel Xeon W-2102 CPU @ 2.90 GHz and 16 GB RAM, running 64-bit Windows 7. The workflow consists of five stages: DFM Generation (0.19 s/realization), Fracture-Coarse Grid Partitioning (0.93 s/realization), Simulation Setup (1.43 s/realization), Flow Simulation (40.4 s/realization), and Upscaling Calculation (17.9 s/realization). Flow Simulation dominates the computational cost, accounting for 65% of total runtime, which is expected given the need to solve pressure equations for accurate effective permeability calculations. This ensemble-based uncertainty quantification demonstrates UpsFrac's capability to efficiently perform Monte Carlo workflows for stochastic DFN analysis, transforming complex discrete fracture systems into stochastic continuum representations while preserving uncertainty information critical for risk assessment in subsurface applications.

5 Limitations and future developments

5.1 Impact of constant aperture assumption on fracture roughness modelling

The constant aperture assumption, while computationally efficient and widely adopted in discrete fracture modelling, represents a significant simplification of natural fracture geometries. Real fractures exhibit complex aperture distributions arising from surface roughness, stress-induced deformation, and mineral precipitation or dissolution processes (Li et al., 2022; Xue et al., 2022). To quantify the impact of this simplification, we conducted a systematic analysis comparing upscaled permeabilities computed using constant versus variable aperture distributions. The test case employs a single

horizontal fracture configuration identical to the validation case (Fig. 9, θ = 0°) with a 2 m × 2 m domain and mean aperture w_0 = 1.2×10⁻⁴ m. Fig. 21a demonstrates the aperture variability along a 2 m fracture for different roughness levels characterized by coefficients of variation (CV) ranging from 0.1 to 0.5, representing mild to severe aperture heterogeneity. The corresponding statistical distributions of these aperture profiles are shown in Fig. 21b through box plots, revealing increasing spread and skewness with higher CV values.
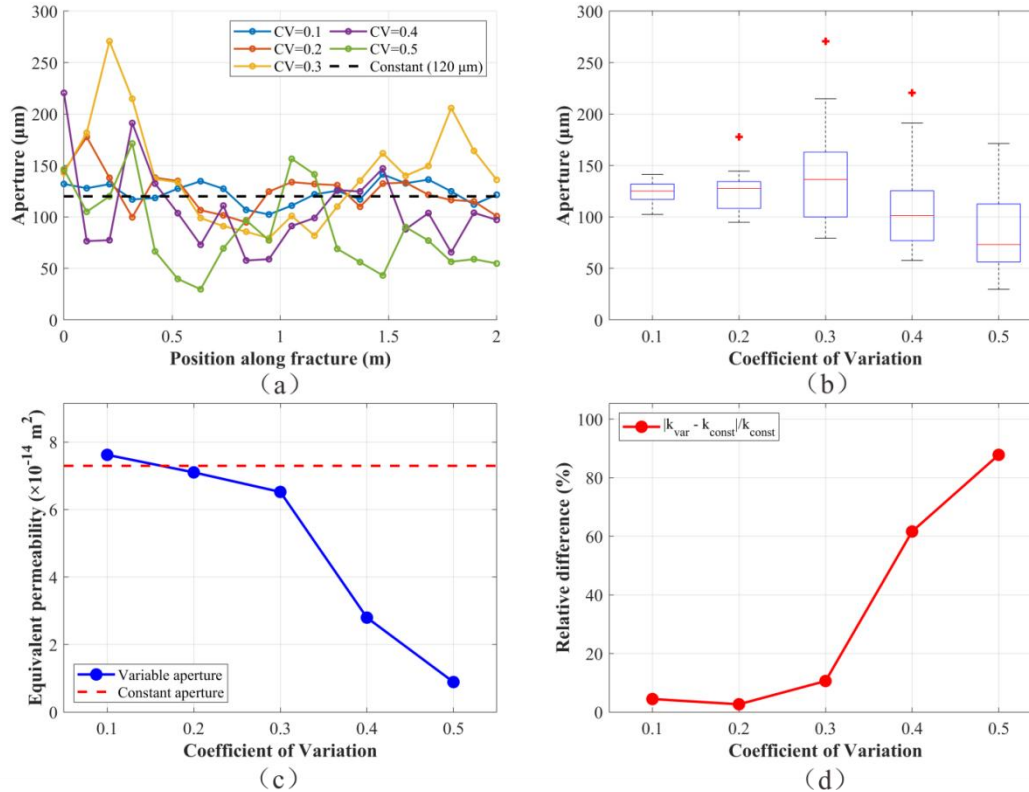
Figure 21: Effects of aperture variability: (a) aperture profiles along a 2 m fracture (CV = 0.1–0.5, mean aperture w_0 = 1.2×10-4 m); (b) aperture statistics (box: IQR; red line: median; whiskers: 1.5×IQR; crosses: outliers); (c) equivalent permeability vs CV (relative to constant aperture); (d) relative error of the constant-aperture assumption.

Our analysis exposes fundamental limitations of the constant-aperture assumption. Although it enables tractable simulations, accuracy degrades markedly for naturally rough fractures. As illustrated in Fig. 21c, the upscaled permeability in the x-direction (k_{xx}) decreases substantially with increasing roughness relative to the constant aperture case. Errors increase nonlinearly with roughness. Figure 21d quantifies this degradation, showing relative errors rising from negligible (<5%) when CV < 0.2 to severe (>60%) when CV > 0.4. This occurs because the arithmetic-mean aperture cannot capture flow channeling, and the cubic law disproportionately amplifies contributions from wider segments while constrictions strongly restrict flow.

These findings have direct implications for reservoir characterization and model selection. For preliminary assessments or systems dominated by smooth, fresh tensile fractures in crystalline rocks or well-sorted sedimentary formations (CV < 0.2), where Fig. 21d indicates errors remain below 5%, the constant-aperture model offers an efficient and sufficiently accurate approximation. In contrast, for highly rough fractures such as sheared zones and mineralized joints, explicitly representing aperture variability is essential for reliable predictions. UpsFrac's modular architecture readily accommodates this extension: supporting rough fractures requires only augmenting fracture property storage and revising local flow calculations, while preserving the existing upscaling framework.

5.2 Three-dimensional model extension roadmap

While the current 2D implementation provides a robust foundation for method validation and pedagogical purposes, extending to 3D is essential for industrial applications. To address industrial needs, we outline a comprehensive roadmap for extending UpsFrac to 3D. Specifically, we will: (i) generalize DFN generation from 2D line fractures to 3D planar polygonal or triangulated fracture surfaces with realistic size, orientation, aperture, and connectivity distributions; (ii) extend MFU to 3D with robust treatment of fracture intersections, complex fracture–matrix exchange, anisotropy, and boundary conditions; and (iii) mitigate the substantially higher computational cost through algorithmic accelerations, including adaptive/octree meshing, hierarchical fracture-surface meshing, algebraic multigrid preconditioning, domain decomposition with parallel CPU/GPU solvers, and graph-based pruning of disconnected subnetworks. Building on our prior 3D upscaling experience (Chen et al., 2018) and established platforms such as ADFNE and MRST, we anticipate that the integration is technically feasible, though computational challenges primarily arise from the cubic scaling of 3D problems—where doubling the grid resolution increases computational cost eightfold. This provides a clear path toward evaluating industrial applicability in complex reservoir systems.

5.3 Accelerating flow-based upscaling

UpsFrac implements a theoretically rigorous flow-based upscaling approach. In practice, the upscaling step requires numerically solving flow in a discrete fracture model, where numerical stability must be considered for complex geometries. Achieving stable and accurate solutions may require adjusting parameters such as the mesh resolution in the fractures and the rock matrix. To prevent failed runs and facilitate correction, grid blocks that contain no fractures or that fail to converge are logged for review; by reviewing these logs, users can refine global template inputs or adjust settings for specific blocks. In the future, data-driven surrogates trained on high-fidelity DFN simulations (e.g., Almajid and Abu-Al-Saud, 2022; Yan et al., 2024) may augment or replace direct solves to further improve robustness and efficiency.

5.4 Integration of alternative upscaling methods

The UpsFrac software applies MFU for calculating equivalent permeability, which is accurate as a flow-based method; other

fast analytical upscaling methods (Ebigbo et al., 2016; Oda, 1985), such as Effective Medium Theory (EMT), can also easily be implemented within the UpsFrac framework to upscale permeability in fractured porous rocks. The software can be further developed to broaden its applicability and improve user convenience. Key areas for improvement include the user interface, software stability, and compatibility with other reservoir simulation tools. This can be achieved through standardization of data formats and the development of API interfaces, which will facilitate broader adoption in industrial settings (Yan et al., 2024).

6 Conclusions

The paper describes a new free and open-source software UpsFrac for modelling and upscaling the permeability of two-dimensional fractured porous rocks with fractal characteristics. The software provides a methodology for creating multiple-scale fractures with varied apertures using both deterministic and stochastic approaches. The complex relations between fracture length, fracture density, and fracture aperture can be easily implemented in the framework of UpsFrac. The software applies the state-of-the-art upscaling method, MFU, which is a flow-based upscaling approach based on the TPFA or MPFA schemes and provides accurate and robust upscaling results.

UpsFrac addresses a critical gap in modelling of fractured porous rocks by providing an integrated open-source platform that seamlessly connects fractal fracture characterization with practical upscaling workflows. The software's key innovations include automated uncertainty quantification through Monte Carlo ensembles, direct DFM-to-EFM coupling without intermediate file conversions, and a modular architecture enabling algorithm substitution. Validation demonstrates exceptional accuracy across diverse geological conditions while achieving significant computational efficiency gains.

The software provides a flexible toolbox for modelling and analyzing fractured porous rocks with complex fracture geometries. The discrete fracture models can be upscaled to calculate equivalent permeability. The software is useful for investigating the heterogeneity and anisotropy of equivalent fracture permeability for fractured porous rocks. The upscaled permeability tensors can serve as input parameters in the equivalent fracture models. All the code and application scripts are available for download.

Author contribution

TC: Conceptualization, Writing-original draft, Software, Investigation, Formal analysis, Funding acquisition. HS: Writing-review & editing, Methodology, Validation, Visualization. YZ: Writing-review & editing, Software, Data curation. FK: Writing-review & editing.

Competing interests

The authors declare that they have no competing interests.

Acknowledgments

We sincerely thank Mohammad Sabah and one anonymous reviewer for their valuable comments and constructive suggestions on the manuscript. Their careful reading and insightful feedback have substantially improved the quality of this paper. This work was funded by the National Natural Science Foundation of China (42002261). We would like to extend our gratitude to the open source software developers related to ADFNE and MRST. We thank Anozie Ebigbo for valuable discussions and constructive suggestions on the manuscript.

Code and data availability

The UpsFrac code is available on GitHub (https://github.com/chentao9330/UpsFrac, last access: 30 September 2025), and version 1.0 is archived on Zenodo (Chen, 2025; https://doi.org/10.5281/zenodo.14674083). The UpsFrac code is published under the GNU General Public License v3.0 (GPL-3.0 license). All input data in this study can be reproduced following the parameters and procedures described in this paper. The example input file used in this study can be found in the example folder of UpsFrac.

References

Alghalandis, Y.F., 2017. ADFNE: Open source software for discrete fracture network engineering, two and three dimensional applications. Computers & Geosciences 102, 1–11. https://doi.org/10.1016/j.cageo.2017.02.002

Almajid, M.M., Abu-Al-Saud, M.O., 2022. Prediction of porous media fluid flow using physics informed neural networks. Journal of Petroleum Science and Engineering 208, 109205. https://doi.org/10.1016/j.petrol.2021.109205

Andrews, B.J., Roberts, J.J., Shipton, Z.K., Bigi, S., Tartarello, M.C., Johnson, G., 2019. How do we see fractures? Quantifying subjective bias in fracture data collection. Solid Earth 10, 487–516. https://doi.org/10.5194/se-10-487-2019

Berre, I., Doster, F., Keilegavlen, E., 2018. Flow in Fractured Porous Media: A Review of Conceptual Models and Discretization Approaches. Transport in Porous Media 130, 215–236. https://doi.org/10.1007/s11242-018-1171-6

Bonnet, E., Bour, O., Odling, N.E., Davy, P., Main, I., Cowie, P., Berkowitz, B., 2001. Scaling of fracture systems in geological media. Reviews of Geophysics 39, 347–383. https://doi.org/10.1029/1999rg000074

Borghini, L., Striglio, G., Bacchiani, G., La Bruna, V., Balsamo, F., Bonini, L., Bezerra, F.H.R., 2024. Fracture analyser: a Python toolbox for the 2D analysis of fracture patterns. https://doi.org/10.3301/ijg.2024.16

Chen, T., 2025. Open-source software for integrating modelling and upscaling permeability for fractured porous rocks: UpsFrac. Zenodo. https://doi.org/10.5281/zenodo.14674083

550   Chen, T., Clauser, C., Marquart, G., Willbrand, K., Büsing, H., 2016. Modeling anisotropic flow and heat transport by using mimetic finite differences. Advances in Water Resources 94, 441–456. https://doi.org/10.1016/j.advwatres.2016.06.006

Chen, T., Clauser, C., Marquart, G., Willbrand, K., Mottaghy, D., 2015. A new upscaling method for fractured porous media. Advances in Water Resources 80, 60–68. https://doi.org/10.1016/j.advwatres.2015.03.009

Chen, T., Clauser, C., Marquart, G., Willbrand, K., Hiller, T., 2018. Upscaling permeability for three-dimensional fractured

555   porous rocks with the multiple boundary method. Hydrogeology Journal, 26(6), 1903-1916.

Cheng, Y., Wong, L.N.Y., 2018. Microscopic Characterization of Tensile and Shear Fracturing in Progressive Failure in Marble. Journal of Geophysical Research: Solid Earth 123, 204–225. https://doi.org/10.1002/2017JB014581

Cook, P.G., Love, A.J., Robinson, N.I., Simmons, C.T., 2005. Groundwater ages in fractured rock aquifers. Journal of Hydrology 308, 284–301. https://doi.org/10.1016/j.jhydrol.2004.11.005

560   Corral, Á., González, Á., 2019. Power Law Size Distributions in Geoscience Revisited. Earth and Space Science 6, 673–697. https://doi.org/10.1029/2018EA000479

Ebigbo, A., Lang, P.S., Paluszny, A., Zimmerman, R.W., 2016. Inclusion-Based Effective Medium Models for the Permeability of a 3D Fractured Rock Mass. Transport in Porous Media 113, 137–158. https://doi.org/10.1007/s11242-016-0685-z

565   Fiori, A., Bellin, A., Cvetkovic, V., De Barros, F.P.J., Dagan, G., 2015. Stochastic modeling of solute transport in aquifers: From heterogeneity characterization to risk analysis. Water Resources Research 51, 6622–6648. https://doi.org/10.1002/2015WR017388

Ghassemi, A., 2012. A Review of Some Rock Mechanics Issues in Geothermal Reservoir Development. Geotechnical and Geological Engineering 30, 647–664. https://doi.org/10.1007/s10706-012-9508-3

570   Gong, L., Wang, J., Gao, S., Fu, X., Liu, B., Miao, F., Zhou, X., Meng, Q., 2021. Characterization, controlling factors and evolution of fracture effectiveness in shale oil reservoirs. Journal of Petroleum Science and Engineering 203, 108655. https://doi.org/10.1016/j.petrol.2021.108655

Gottron, D., Henk, A., 2021. Upscaling of fractured rock mass properties – An example comparing Discrete Fracture Network (DFN) modeling and empirical relations based on engineering rock mass classifications. Engineering Geology 294,

575   106382. https://doi.org/10.1016/j.enggeo.2021.106382

Gu, X., Rempe, D.M., Dietrich, W.E., West, A.J., Lin, T.-C., Jin, L., Brantley, S.L., 2020. Chemical reactions, porosity, and microfracturing in shale during weathering: The effect of erosion rate. Geochimica et Cosmochimica Acta 269, 63–100. https://doi.org/10.1016/j.gca.2019.09.044

Gudmundsson, A., 2011. Rock Fractures in Geological Processes. Cambridge University Press.

580   Hardebol, N.J., Bertotti, G., 2013. DigiFract: A software and data model implementation for flexible acquisition and processing of fracture data from outcrops. Computers & Geosciences 54, 326–336. https://doi.org/10.1016/j.cageo.2012.10.021

Healy, D., Rizzo, R.E., Cornwell, D.G., Farrell, N.J.C., Watkins, H., Timms, N.E., Gomez-Rivas, E., Smith, M., 2017. FracPaQ: A MATLABTM toolbox for the quantification of fracture patterns. Journal of Structural Geology 95, 1–16.

585   https://doi.org/10.1016/j.jsg.2016.12.003

HosseiniMehr, M., Tomala, J.P., Vuik, C., Kobaisi, M.A., Hajibeygi, H., 2022. Projection-based embedded discrete fracture model (pEDFM) for flow and heat transfer in real-field geological formations with hexahedral corner-point grids. Advances in Water Resources 159, 104091. https://doi.org/10.1016/j.advwatres.2021.104091

Hyman, J.D., Karra, S., Makedonska, N., Gable, C.W., Painter, S.L., Viswanathan, H.S., 2015. dfnWorks: A discrete
590   fracture network framework for modeling subsurface flow and transport. Computers & Geosciences, 84, 10-19. https://doi.org/10.1016/j.cageo.2015.08.001

Hyman, J.D., Aldrich, G., Viswanathan, H., Makedonska, N., Karra, S., 2016. Fracture size and transmissivity correlations: Implications for transport simulations in sparse three-dimensional discrete fracture networks following a truncated power law distribution of fracture size. Water Resources Research 52, 6472–6489. https://doi.org/10.1002/2016wr018806

595   Keilegavlen, E., Berge, R., Fumagalli, A., Starnoni, M., Stefansson, I., Varela, J., Berre, I., 2021. PorePy: an open-source software for simulation of multiphysics processes in fractured porous media. Computational Geosciences 25, 243–265. https://doi.org/10.1007/s10596-020-10002-5

Keller, J., Rath, V., Bruckmann, J., Mottaghy, D., Clauser, C., Wolf, A., Seidler, R., Bücker, H.M., Klitzsch, N., 2020. SHEMAT-Suite: An open-source code for simulating flow, heat and species transport in porous media. SoftwareX 12,
600   100533. https://doi.org/10.1016/j.softx.2020.100533

Klimczak, C., Schultz, R.A., Parashar, R., Reeves, D.M., 2010. Cubic law with aperture-length correlation: implications for network scale fluid flow. Hydrogeology Journal 18, 851–862. https://doi.org/10.1007/s10040-009-0572-6

Kolditz, O., Bauer, S., Bilke, L., Böttcher, N., Delfs, J.O., Fischer, T., Görke, U.J., Kalbacher, T., Kosakowski, G., McDermott, C.I., Park, C.H., Radu, F., Rink, K., Shao, H., Shao, H.B., Sun, F., Sun, Y.Y., Singh, A.K., Taron, J., Walther,
605   M., Wang, W., Watanabe, N., Wu, Y., Xie, M., Xu, W., Zehner, B., 2012. OpenGeoSys: an open-source initiative for numerical simulation of thermo-hydro-mechanical/chemical (THM/C) processes in porous media. Environmental Earth Sciences 67, 589–599. https://doi.org/10.1007/s12665-012-1546-x

Lang, P.S., Paluszny, A., Zimmerman, R.W., 2014. Permeability tensor of three-dimensional fractured porous rock and a comparison to trace map predictions. Journal of Geophysical Research: Solid Earth 119, 6288–6307.
610   https://doi.org/10.1002/2014jb011027

Li, Z., Sherman, C.S., Reagan, M.T., Moridis, G.J., Morris, J.P., 2022. Effects of Heterogeneous Fracture Aperture on Multiphase Production from Shale Reservoirs. Transport in Porous Media 144, 797–823. https://doi.org/10.1007/s11242-022-01841-0

Lie, K. A., 2019. An Introduction to Reservoir Simulation Using MATLAB/GNU Octave: User Guide for the MATLAB
Reservoir Simulation Toolbox (MRST). Cambridge University Press, Cambridge.

Liu, Z., Reynolds, A.C., n.d. History Matching an Unconventional Reservoir with a Complex Fracture Network.

MacQuarrie, K.T.B., Mayer, K.U., 2005. Reactive transport modeling in fractured rock: A state-of-the-science review.
Earth-Science Reviews 72, 189–227. https://doi.org/10.1016/j.earscirev.2005.07.003

Marinos, Vassilis., Carter, Trevor.G., 2018. Maintaining geological reality in application of GSI for design of engineering
structures in rock. Engineering Geology 239, 282–297. https://doi.org/10.1016/j.enggeo.2018.03.022

Massart, B., Paillet, M., Henrion, V., Sausse, J., Dezayes, C., Genter, A., Bisset, A., 2010. Fracture characterization and
stochastic modeling of the granitic basement in the HDR Soultz Project (France), in: Proceedings World Geothermal
Congress 2010. Bali, Indonesia.

McDermott, C., Kolditz, O., 2006. Geomechanical model for fracture deformation under hydraulic, mechanical and thermal
loads. Hydrogeology Journal 14, 485–498. https://doi.org/10.1007/s10040-005-0455-4

Mejia, C., Roehl, D., Rueda, J., Quevedo, R., 2021. A new approach for modeling three-dimensional fractured reservoirs
with embedded complex fracture networks. Computers and Geotechnics 130, 103928.
https://doi.org/10.1016/j.compgeo.2020.103928

Molnar, P., Anderson, R.S., Anderson, S.P., 2007. Tectonics, fracturing of rock, and erosion. Journal of Geophysical
Research: Earth Surface 112. https://doi.org/10.1029/2005JF000433

Myers, T., 2012. Potential Contaminant Pathways from Hydraulically Fractured Shale to Aquifers. Groundwater 50, 872–
882. https://doi.org/10.1111/j.1745-6584.2012.00933.x

Neuman, S.P., 2005. Trends, prospects and challenges in quantifying flow and transport through fractured rocks.
Hydrogeology Journal 13, 124–147.

Oda, M., 1985. Permeability tensor for discontinuous rock masses. Géotechnique 35, 483–495.
https://doi.org/10.1680/geot.1985.35.4.483

Odling, N.E., Roden, J.E., 1997. Contaminant transport in fractured rocks with significant matrix permeability, using natural
fracture geometries. Journal of Contaminant Hydrology 27, 263–283. https://doi.org/10.1016/S0169-7722(96)00096-4

Olson, J.E., 2003. Sublinear scaling of fracture aperture versus length: An exception or the rule? Journal of Geophysical
Research: Solid Earth 108. https://doi.org/10.1029/2001jb000419

Ovaskainen, N., 2023. fractopo: A Python package for fracture network analysis. Journal of Open Source Software 8, 5300.
https://doi.org/10.21105/joss.05300

Palamakumbura, R., Krabbendam, M., Whitbread, K., Arnhardt, C., 2020. Data acquisition by digitizing 2-D fracture
networks and topographic lineaments in geographic information systems: further development and applications. Solid Earth
11, 1731–1746. https://doi.org/10.5194/se-11-1731-2020

Rajeh, T., Ababou, R., Marcoux, M., Cañamon, I., 2019. Fast Upscaling of the Hydraulic Conductivity of Three-Dimensional Fractured Porous Rock for Reservoir Modeling. Mathematical Geosciences 51, 1037–1074. https://doi.org/10.1007/s11004-019-09785-w

Renard, P., Ababou, R., 2022. Equivalent Permeability Tensor of Heterogeneous Media: Upscaling Methods and Criteria (Review and Analyses). Geosciences 12, 269. https://doi.org/10.3390/geosciences12070269

Sandve, T.H., Berre, I., Nordbotten, J.M., 2012. An efficient multi-point flux approximation method for Discrete Fracture–Matrix simulations. Journal of Computational Physics 231, 3784–3800. https://doi.org/10.1016/j.jcp.2012.01.023

Schultz, R.A., Soliva, R., 2012. Propagation energies inferred from deformation bands in sandstone. International Journal of Fracture 176, 135–149. https://doi.org/10.1007/s10704-012-9730-2

Snow, D.T., 1969. Anisotropie permeability of fractured media, Water Resources Research, 5(6), 1273-1289.

Srinivasan, G., Hyman, J.D., Osthus, D.A., Moore, B.A., O'Malley, D., Karra, S., Rougier, E., Hagberg, A.A., Hunter, A., Viswanathan, H.S., 2018. Quantifying Topological Uncertainty in Fractured Systems using Graph Theory and Machine Learning. Scientific Reports 8, 11665. https://doi.org/10.1038/s41598-018-30117-1

Vermilye, J.M., Scholz, C.H., 1995. Relation between vein length and aperture. Journal of Structural Geology 17, 423–434. https://doi.org/10.1016/0191-8141(94)00058-8

Viswanathan, H.S., Ajo-Franklin, J., Birkholzer, J.T., Carey, J.W., Guglielmi, Y., Hyman, J.D., Karra, S., Pyrak-Nolte, L.J., Rajaram, H., Srinivasan, G., Tartakovsky, D.M., 2022. From Fluid Flow to Coupled Processes in Fractured Rock: Recent Advances and New Frontiers. Reviews of Geophysics 60, e2021RG000744. https://doi.org/10.1029/2021RG000744

Wang, Q., Zhang, L., Yu, Q., Li, H., 2023. Existence analysis of hydraulic conductivity representative elementary volume in fractured rocks based on three-dimensional discrete fracture network method. Computers and Geotechnics 164, 105829.

Welch, M. J., Lüthje, M., Oldfield, S. J., 2022. DFN Generator v2. 0: A new tool to model the growth of large-scale natural fracture networks using fundamental geomechanics. Geoscientific Model Development Discussions, 2022, 1-42.

Weismüller, C., Prabhakaran, R., Passchier, M., Urai, J.L., Bertotti, G., Reicherter, K., 2020. Mapping the fracture network in the Lilstock pavement, Bristol Channel, UK: manual versus automatic. Solid Earth 11, 1773–1802. https://doi.org/10.5194/se-11-1773-2020

Wong, D., Doster, F., Geiger, S., 2021. Embedded Discrete Fracture Models, in: Lie, K.-A., Møyner, O. (Eds.), Advanced Modeling with the MATLAB Reservoir Simulation Toolbox. Cambridge University Press, Cambridge, pp. 375–408. https://doi.org/10.1017/9781009019781.015

Xu, C., Dowd, P., 2010. A new computer code for discrete fracture network modelling. Computers & Geosciences 36, 292–301. https://doi.org/10.1016/j.cageo.2009.05.012

Xue, K., Zhang, Z., Zhong, C., Jiang, Y., Geng, X., 2022. A fast numerical method and optimization of 3D discrete fracture network considering fracture aperture heterogeneity. Advances in Water Resources 162, 104164. https://doi.org/10.1016/j.advwatres.2022.104164

Yan, M., Huang, C., Bienstman, P., Tino, P., Lin, W., Sun, J., 2024. Emerging opportunities and challenges for the future of reservoir computing. Nature Communications 15, 2056. https://doi.org/10.1038/s41467-024-45187-1

Yan, X., Lin, J., Wang, S., Zhang, Z., Liu, P., Sun, S., Yao, J., Zhang, K., 2024. Physics-informed neural network simulation of two-phase flow in heterogeneous and fractured porous media. Advances in Water Resources 189, 104731. https://doi.org/10.1016/j.advwatres.2024.104731

Zijl, W., Stam, J.M.T., 1992. Modeling permeability in imperfectly layered porous media. I. Derivation of block-scale permeability tensor for thin grid-blocks. Mathematical Geology 24, 865–883. https://doi.org/10.1007/BF00894656

Zoback, M.D., Barton, C.A., Brudy, M., Castillo, D.A., Finkbeiner, T., Grollimund, B.R., Moos, D.B., Peska, P., Ward, C.D., Wiprut, D.J., 2003. Determination of stress orientation and magnitude in deep wells. International Journal of Rock Mechanics and Mining Sciences, Special Issue of the IJRMMS: Rock Stress Estimation ISRM Suggested Methods and Associated Supporting Papers 40, 1049–1076. https://doi.org/10.1016/j.ijrmms.2003.07.001

Appendix A: Algorithm Implementation and Technical Details

A.1 Core Upscaling Algorithm

```
Algorithm: UpsFrac Equivalent Permeability Upscaling
Main input:
  - Domain parameters: L (domain size), nx, ny (grid numbers), d (grid block size)
  - DFN parameters: n (fracture number), l_min, l_max, α (power-law exponent)
  - Matrix permeability: k_matrix
  - Number of realizations: num_real

Output:
  - Equivalent permeability tensor K_eq[i,j] for each grid block

Main Procedure:

1. DFN Generation (DiscreteFractureModeling.m):
    FOR each realization r = 1 to num_real:
        Generate n fractures with:
            - Length l[i] ~ power_law(l_min, l_max, α)
            - Aperture a[i] = γ × l[i]^D
            - Random position (x,y) and orientation θ
        SAVE fracture geometries to frac_0_r.txt

2. Grid Discretization (SubDivideToGrid.m):
    FOR each fracture f in DFN:
        FOR each grid block (i,j) where i∈[1,nx], j∈[1,ny]:
            IF fracture f intersects grid block (i,j):
                Clip fracture to grid boundaries
                Adjust corner points by move_ratio to avoid meshing issues
                STORE clipped segment in resu_0_r.txt with:
                    - Grid ID = i + (j-1)×nx
                    - Endpoints (x1,y1,x2,y2)
                    - Aperture w

3. DFM Simulation Setup (DiscreteFractureInput.m):
    FOR each grid block g with fractures:
        Create MRST input file s[g].m:
            - Define unstructured triangular mesh
            - Embed fractures as lower-dimensional elements
            - Set matrix permeability = k_matrix
            - Set fracture permeability = w²/12

4. Flow Simulation (GridDFMSimu.m):
    FOR each grid block g:
        FOR each pressure gradient direction d ∈ {x, y}:
            Apply linear boundary conditions:
                IF d = x: p_left = L, p_right = 0, p_top/bottom = linear
```

```
740              IF d = y: p_top = L, p_bottom = 0, p_left/right = linear
             Solve flow equation: ∇·(k∇p) = 0
             SAVE boundary fluxes q[boundary,d]

   5. Equivalent Permeability Calculation (CalcuKeq.m):
745    FOR each grid block g:
           FOR each boundary b ∈ {left, right, top, bottom}:
              Calculate total flux:
              q_total[b] = Σ(q_matrix[b] + q_fracture[b]·n)
              where n = normal vector
750
       Compute K_eq components using Darcy's law:
           From x-direction flow:
              K_xx = q_x,out × d / (Δp × A)
              K_yx = q_y,out × d / (Δp × A)
755        From y-direction flow:
              K_xy = q_x,out × d / (Δp × A)
              K_yy = q_y,out × d / (Δp × A)

       Validate and correct:
760        IF K_ii ≤ 0 OR K_ii > threshold:
              K_ii = k_matrix
           IF |K_ij| < k_matrix:
              K_ij = 0

765        SAVE K_eq to epcomf.txt

   END Algorithm
```

A.2 Implementation Structure

770

Table A1. Computational modules and their implementation

Module	Implementation File	Primary Function	Key Parameters
DFN Generation	DiscreteFractureModeling.m	Generate stochastic fracture networks	num_real, n, α, l_min, l_max
Grid Partitioning	SubDivideToGrid.m	Clip and assign fractures to grid blocks	nx, ny, move_ratio
Simulation Setup	DiscreteFractureInput.m	Create MRST-compatible DFM models	mesh_size, k_matrix
Flow Solver	GridDFMSimu.m	Execute batch flow simulations	solver_type (TPFA/MPFA)
Upscaling	CalcuKeq.m	Calculate equivalent permeability tensors	tolerance, validation_threshold

Table A2. Data structure specifications

Data Type	Format	Structure	Description
Fracture geometry	ASCII text	5 columns: x1, y1, x2, y2, aperture	Initial fracture network definition
Grid-fracture mapping	ASCII text	grid_ID, fracture segments	Fractures assigned to each grid block
Flux output	ASCII text	boundary_ID, flux_x, flux_y	Computed boundary fluxes
Permeability tensor	ASCII text	kxx, kxy, kyx, kyy	Final upscaled properties